ACS APPLIED MATERIALS & INTERFACES

Research Article

Cite This: ACS Appl. Mater. Interfaces XXXX, XXX, XXX−XXX

www.acsami.org

Wearable, Ultrawide-Range, and Bending-Insensitive Pressure Sensor Based on Carbon Nanotube Network-Coated Porous Elastomer Sponges for Human Interface and Healthcare Devices

Seunghwan Kim,[†] Morteza Amjadi,[‡] Tae-Ik Lee,[†] Yongrok Jeong,[†] Donguk Kwon,[†] Min Seong Kim,[†] Kyuyoung Kim,[†] Taek-Soo Kim,[†] Yong Suk Oh,*[,†,§] and Inkyu Park*[,†]

[†]Department of Mechanical Engineering, Korea Advanced Institute of Science and Technology (KAIST), 291 Daehak-ro, Yuseong-gu, Daejeon 305-701, South Korea

[‡]Physical Intelligence Department, Max-Planck Institute for Intelligent Systems, Heisenbergstrasse 3, Stuttgart 70569, Germany

[§]Center for Bio-Integrated Electronics (CBIE), Northwestern University, Evanston, Illinois 60208, United States

Supporting Information

ABSTRACT: Flexible and wearable pressure sensors have attracted a tremendous amount of attention due to their wider applications in human interfaces and healthcare monitoring. However, achieving accurate pressure detection and stability against external stimuli (in particular, bending deformation) over a wide range of pressures from tactile to body weight levels is a great challenge. Here, we introduce an ultrawide-range, bending-insensitive, and flexible pressure sensor based on a carbon nanotube (CNT) network-coated thin porous elastomer sponge for use in human interface devices. The integration of the CNT networks into three-dimensional microporous elastomers provides high deformability and a large change in contact between the conductive CNT networks due to the presence of micropores, thereby improving the sensitivity compared with that obtained using CNT-embedded solid elastomers. As electrical pathways are continuously generated up to high compressive strain (~80%), the pressure sensor shows an ultrawide pressure sensing range (10 Pa to 1.2 MPa) while maintaining favorable sensitivity (0.01−0.02 kPa^{-1}) and linearity ($R^2 \sim 0.98$). Also, the pressure sensor exhibits excellent electromechanical stability and insensitivity to bending-induced deformations. Finally, we demonstrate that the pressure sensor can be applied in a flexible piano pad as an entertainment human interface device and a flexible foot insole as a wearable healthcare and gait monitoring device.

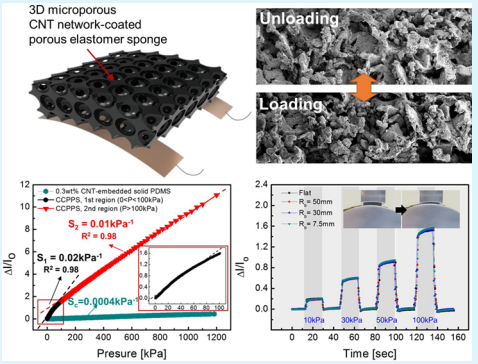

KEYWORDS: *carbon nanotube, microporous elastomer, flexible pressure sensor, ultrawide pressure range, bending insensitivity, human interface device*

INTRODUCTION

Flexible and wearable pressure sensors have received a tremendous amount of attention due to their great potential for a variety of applications, including artificial electronic skins,[1−4] soft robotics,[5−7] healthcare monitoring and diagnosis,[8−11] energy harvesting,[12−14] and human interface devices.[15,16] Next-generation flexible pressure sensors are required to precisely detect a wide range of pressures (low-pressure regime of 0−10 kPa, medium-pressure regime of 10−100 kPa, and high-pressure regime of >100 kPa) with high sensitivity and reliability for use in human body monitoring systems.[10,17]

In general, flexible pressure sensors are mainly divided into resistive, capacitive, and piezoelectric types according to the pressure sensing mechanisms. Among them, resistive pressure sensors have been intensively investigated because of their advantages such as simple device structures, easy signal readout, and high pixel resolution.[10,18] Conventionally, flexible pressure sensors have been fabricated using a method for embedding conductive nanomaterials [e.g., carbon blacks, carbon nanotubes (CNTs), etc.] into a polymer or elastomer matrix [e.g., polydimethylsiloxane (PDMS), Ecoflex, polyurethane, etc.]. These types of pressure sensors, however, suffered from low sensitivity and poor hysteresis over wide ranges of pressure due to an imperfect recovery of the conductive nanomaterial networks and inherent viscoelasticity of the matrix materials, thereby limiting their practical applications.[7,19,20] Several strategies have been proposed to improve the performance of flexible pressure sensors using a variety of two-dimensional (2D) micro/nanostructured active layers, including conductive polymer-coated micropyramid arrays,[21] electrospun nanofiber-based thin films,[22] and

Received: May 1, 2019
Accepted: June 10, 2019
Published: June 10, 2019

DOI: 10.1021/acsami.9b07636
ACS Appl. Mater. Interfaces XXXX, XXX, XXX−XXX

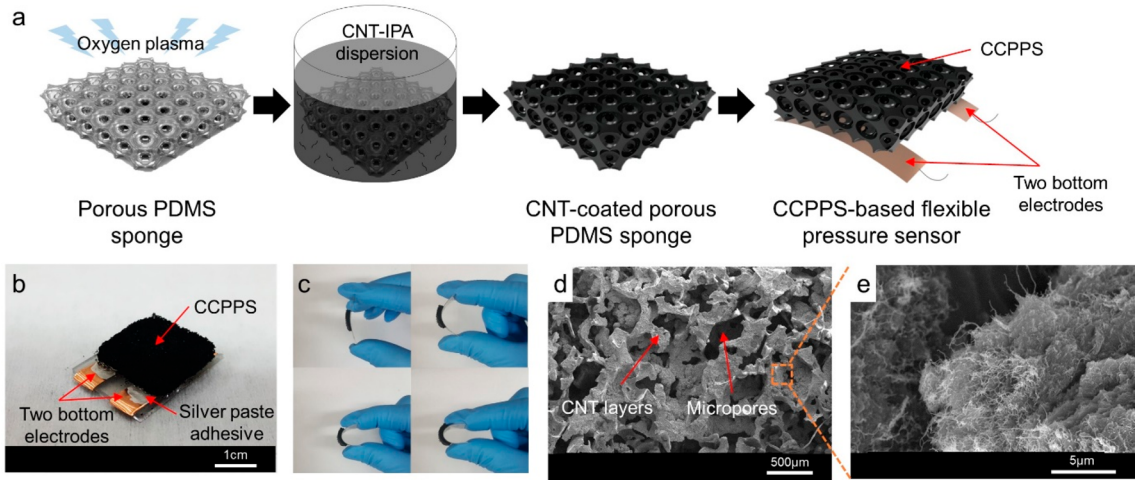

Figure 1. Fabrication and morphology of a CCPPS-based flexible pressure sensor. (a) Schematic illustration of the overall fabrication procedures of the pressure sensor. (b) Photographic image of the pressure sensor composed of a CCPPS as an active layer and two bottom electrodes. (c) Photographic images of the pressure sensor under bent conditions, showing excellent flexibility and structural durability. (d) SEM image of the surface morphology of the CCPPS. (e) Magnified SEM image of CNT layers coated on the porous PDMS backbone, forming conductive networks.

assembly of two interlocked metal-deposited nanofiber arrays.[23] The flexible pressure sensors based on the 2D micro/nanostructured active layers showed excellent sensitivity and quick responses in a low pressure range (generally, <10 kPa) owing to fine contacts between the conductive micro/nanostructures. However, they suffered from expensive, time-consuming, and complicated process steps (e.g., photolithography, etching, and electrospinning). More recently, more efficient, simple, and scalable methods such as biomaterial replicating,[24] ultraviolet (UV) surface modification,[25] laser micro engineering,[26] and conductive microsphere-based film formation[27,28] were suggested for the fabrication of the 2D micro/nanostructured surfaces. However, they still exhibit only small ranges of measurable pressure (<2 or <50 kPa) due to the limited deformation of the 2D micro/nanostructures, which is not suitable for pressure sensing over a large dynamic range.

Alternatively, microscale porous sponge-like materials combined with three-dimensional (3D) conductive networks have been suggested as the active layers of the flexible pressure sensors due to both electrical conductivity and mechanical durability. The 3D conductive sponge-like active layers were typically fabricated using a coating process or a direct synthesis of the conductive nanomaterials (e.g., metal nanowires, graphenes, CNTs, etc.) on porous backbones. For example, highly sensitive pressure sensors based on gold nanowire-coated fabric papers,[29] graphene-coated microfractured polyurethane films,[30] reduced graphene oxide (synthesized by chemical vapor deposition)-coated PDMS foams,[31] and CNT/silver nanoparticle-coated commercial sponges[32] have been reported. Among them, CNT-coated porous PDMS sponges are one of the most promising candidates for use in human interface applications because of the intrinsic flexibility, the skin-like modulus of the PDMS sponge, and the high electrical conductivity of the CNTs. A highly porous and compressible CNT-PDMS sponge fabricated using a simple and cost-effective sugar template-assisted technique was first developed by Han et al.[33] Also, a pressure sensor based on a CNT-PDMS sponge, reported by Iglio et al., showed pressure sensing capability at pressures up to the medium-pressure regime.[34] However, the CNT-PDMS sponge-based pressure sensors have not yet been integrated into human interface devices. There are two important challenges for use in practical human interface applications. First, various sensing parameters (e.g., sensitivity, hysteresis, dynamic response, etc.) of the pressure sensors should be evaluated over a wide range of dynamic pressure. Second, the stability of the pressure sensors should be maintained even under unintended stimuli (in particular, bending deformation).[35]

Herein, we introduce an ultrawide-range, bending-insensitive, and flexible resistive pressure sensor based on a CNT network-coated thin porous PDMS sponge (CCPPS) integrated with two bottom electrodes for use in human interface devices. To investigate its suitability in practical applications, pressure sensing performances of the CCPPS-based pressure sensor were evaluated under static and dynamic conditions. The CCPPS-based pressure sensor exhibited an ultrawide pressure sensing range from 10 Pa to 1.2 MPa while maintaining a favorable sensitivity without a dramatic degradation due to continuous generation of electrical pathways with contact between the serially stacked CNT-coated micropores even over wide compression levels (~80%). Reversible, instant, and robust closure/opening behavior of the micropores within the CCPPS led to low hysteresis, a good dynamic response, and the long-term reliability of the pressure sensor. Also, the CCPPS-based pressure sensor exhibited a bending-insensitive pressure sensing capability, which can lead to an accurate detection of the normal pressure even on curved or dynamic surfaces. To the best of our knowledge, this is the first study of the properties of nanomaterial-coated porous sponge-based pressure sensors under various bent conditions. Finally, the utility of the CCPPS-based flexible pressure sensor was demonstrated for a flexible piano pad and a flexible foot insole.

RESULTS AND DISCUSSION

Figure 1a shows a schematic illustration of the overall fabrication procedures of a flexible resistive pressure sensor, which is composed of a CNT network-coated thin porous PDMS sponge (CCPPS) and two bottom electrodes. The CCPPS was fabricated via the following steps (detailed information in the Experimental Section): (1) fabrication of

DOI: 10.1021/acsami.9b07636
ACS Appl. Mater. Interfaces XXXX, XXX, XXX−XXX

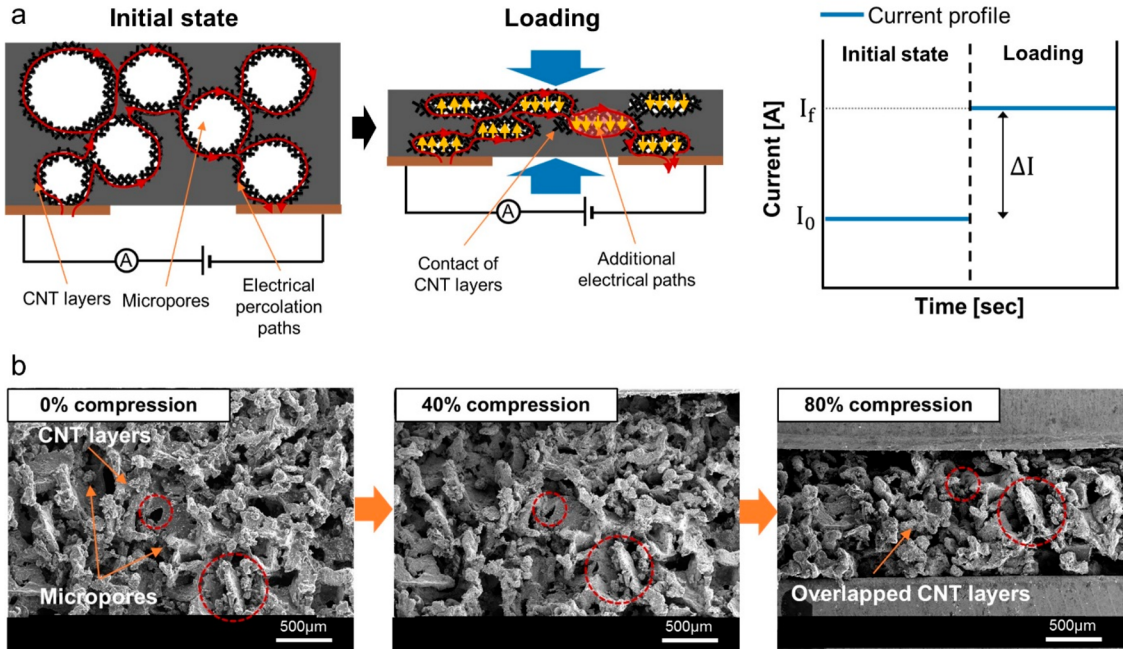

Figure 2. (a) Schematic illustration of the pressure sensing mechanism of the CCPPS-based flexible pressure sensor. An increase in current from I_0 to I_f is induced by additional contact between CNT networks under compressive loading. (b) Cross-sectional SEM images of the CCPPS at compressions of 0%, 40%, and 80%, showing the formation of overlapped CNT layers upon compression of the CCPPS.

a porous PDMS sponge (PSS) using a sugar template, (2) oxygen plasma treatment of the PPS, and (3) CNT coating of the plasma-treated PPS using a dip-coating method for the preparation of a CCPPS (Figure S1a). Panels b and c of Figure S1 show photographic images of the PPS and the CCPPS, respectively. The white color of the PPS was changed to black due to the deposition of the CNTs. In Figure S1d, a slice of the CCPPS cut in half shows that the CNTs were evenly coated inside the PPS. Figure 1b shows a photographic image of the CCPPS-based pressure sensor. It should be noted that the two bottom electrodes are designed for efficient and stable integration of the 3D sensors to 2D electrical circuits for practical human interface applications. Moreover, the pressure sensor with a thickness of <3 mm provides excellent flexibility, which is one of the import factors for human monitoring and wearable applications, as shown in Figure 1c. The pressure sensor was not damaged under various bent conditions. In panels d and e of Figure 1, a scanning electron microscopy (SEM) image and a magnified SEM image show that the surface morphology of the CCPPS has a porous configuration. The size of the micropores is distributed in the range of 300−500 μm, and the porosity was calculated as 73 ± 0.6% (detailed information in Table S1). By comparing the SEM images of the surface morphology of the CCPPS and a bare porous PDMS backbone (Figure S1e), we concluded that complex CNT layers were coated on the 3D-interconnected micropores, which resulted in the formation of conductive networks. In the micro computed tomography (micro CT) image (Movie S1), we observed that the micropores were consistently distributed over the entire volume of the CCPPS.

Figure 2a shows a schematic illustration of the pressure sensing mechanism of the CCPPS-based flexible pressure sensor. An initial current (I_0) flows through electrical percolation paths along the 3D-interconnected CNT networks (red arrow). Under compressive loading, the current increases from I_0 to I_f due to additional electrical paths (yellow arrow) according to an increase in the contact area between the CNT networks during the gradual closure of the micropores. In Figure 2b, cross-sectional SEM images of the CCPPS at compressions of 0%, 40%, and 80% clearly show the formation of overlapped CNT layers upon compression of the CCPPS (the same regions are marked with red circles). Movie S2 shows a gradual geometrical change in the microporous configuration of the CCPPS during several compression/release cycles (0%−80%−0%) in more detail. It should be noted that even at compressions of >60%, the new electrical paths between the CNT networks were continuously generated owing to the presence of the relatively small remaining micropores, which can lead to a sufficient current change even in a high pressure range. Figure S2a shows reversible closure/opening behavior of the micropores with elastic deformation of PDMS bridges surrounding the micropores. Also, almost perfect recovery of the initial states without noticeable structural changes after several compression/release cycles is shown in Figure S2b. In Figure S3a, the CCPPS exhibited a negligible barreling phenomenon, which is a lateral volume expansion, up to a compression of 80%, which originated from the microporous structure, unlike the solid elastomer. The antibarreling property of the CCPPS can lead to the prevention of electrical and physical interference between adjacent sensors for high-resolution array configurations. To prove this property, a one-dimensional (1D) array with six sensors (gap between the sensors of 1 mm) was fabricated as shown in Figure S3b. The sensors were simultaneously compressed by rods by the following procedures: (1) each sensor (S1, S2, ..., S6), (2) two sensors (S2 with S4 or S4 with S6), and (3) two adjacent sensors (S2 with S3 or S5 with S6). Figure S3c and Movie S3 clearly show that each sensor can accurately measure the local pressure without electrical and physical interference with neighboring sensors.

The performance factors of the CCPPS-based flexible pressure sensor that are important for practical applications

DOI: 10.1021/acsami.9b07636
ACS Appl. Mater. Interfaces XXXX, XXX, XXX−XXX

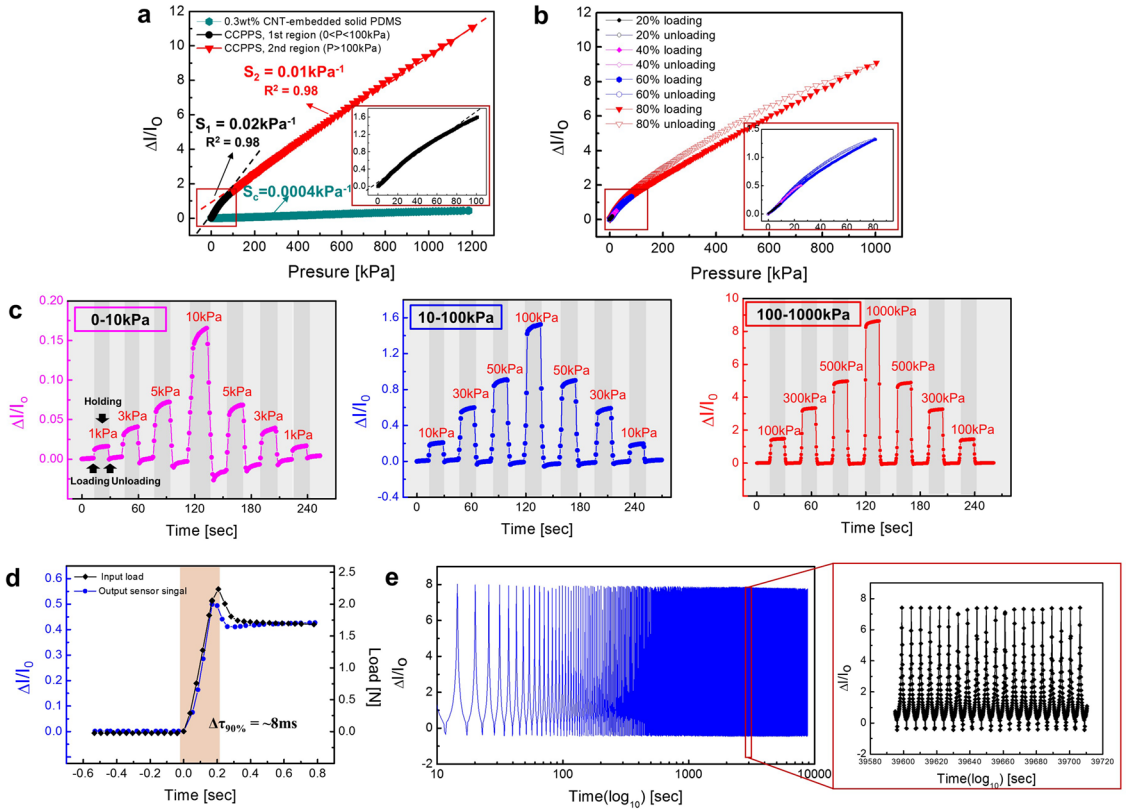

Figure 3. Performance of a CCPPS-based flexible pressure sensor. (a) Pressure response curves of the pressure sensor based on the CCPPS and a CNT-embedded solid PDMS. (b) Hysteresis characteristics of the pressure sensor at various compression levels. (c) Dynamic responses of the pressure sensor at different pressure levels: 0−10, 10−100, and 100−1000 kPa. (d) Transient response of the pressure sensor under a step loading. (e) Long-term reliability of the pressure sensor during 10000 repetitive compression/release (ε_c = 0−75%) cycles.

to human interface devices were systematically evaluated under various static and dynamic loading conditions. Figure 3a compares normalized current changes ($\Delta I/I_0$) as a function of the applied pressure of the pressure sensors based on the CCPPS and a CNT-embedded solid PDMS in a pressure range of $\lesssim$1.2 MPa. The sensitivity is defined as $S = \delta(\Delta I/I_0)/\delta P$, where P denotes the applied pressure and I_0 and ΔI are the initial current and the change in current, respectively. It is noted that the curve of P versus $\Delta I/I_0$ of the CCPPS-based pressure sensor is classified into two regions according to sensitivity. In the first region [0 kPa $\leq P \leq$ 100 kPa, 0% $\leq$ compressive strain (ε_c) $\leq$ 60%, black curve], the CCPPS-based pressure sensor exhibited a sensitivity (S_1) of ~0.02 kPa^{-1}, which is much higher than that of the pressure sensor based on the CNT-embedded solid PDMS (S_c of ~0.0004 kPa^{-1}, green curve). The improvement in sensitivity in the low pressure range is based on the following characteristics of the microporous configuration of the CCPPS: (i) a large increase in the level of contact between the 3D-interconnected CNT networks deposited on the micropores and (ii) low mechanical stiffness due to the presence of the micropores [~30 times lower than that of the CNT-embedded solid PDMS (Figure S4a)] that induce more compressive deformability. These factors can generate large changes in current even under weak external forces. In the second region (100 kPa $\leq P \leq$ 1.2 MPa, 60% $\leq \varepsilon_c \leq$ 80%, red curve), the CCPPS-based pressure sensor exhibited a sensitivity (S_2) of ~0.01 kPa^{-1}, which is lower than S_1 due to gradual closure of the micropores. However, we noticed that a dramatic saturation of the sensitivity was not observed, because new contacts between the CNT networks were continuously created over the wide pressure range (as already observed in Movie S2). The value of S_2 is still higher than those of previously reported pressure sensors working in the high pressure range (0.0009 and 0.0023 kPa^{-1}, etc.).[31,36,37] A high linearity (R^2 ~ 0.98) was also shown over the entire pressure range. Furthermore, to investigate the detection limit of the pressure sensor, precisely controlled input loads of 0.2gf and 1gf were repeatedly applied. Figure S4b shows the detection capability of ultralow pressure levels (10 and 50 Pa) without significant interference from the noise. Accordingly, the CCPPS-based pressure sensor exhibits an ultrawide sensing range from ultralow to high pressures (10 Pa to 1.2 MPa) that covers the whole human tactile and body weight levels, with favorable sensitivity (0.01−0.02 kPa^{-1}) maintained. As shown in Figure S4c, there was no noticeable difference between pressure responses at different compression rates from 0.2 to 1.0 mm/s. This result indicates that the pressure responses of the CCPPS-based pressure sensor would not vary under diverse dynamic stimuli. Figure 3b shows the hysteresis characteristics of the CCPPS-based pressure sensor for various compression levels of 20%, 40%, 60%, and 80%. The pressure sensor exhibited low hysteresis (7.3% for 0−100 kPa and 5.7% for 0−1000 kPa) with a complete recovery of the initial states over the ultrawide pressure range up to ~1 MPa, which originates from the reversible closure/opening behavior of the micropores of the CCPPS (as already shown in Figure S2). Moreover, as shown in Figure 3c, the dynamic sensing properties of the CCPPS-based pressure sensor were evaluated under several loading/holding/unloading dynamic cycles at different pressure levels of 0−10, 10−100, and 100−1000 kPa.

DOI: 10.1021/acsami.9b07636
ACS Appl. Mater. Interfaces XXXX, XXX, XXX−XXX

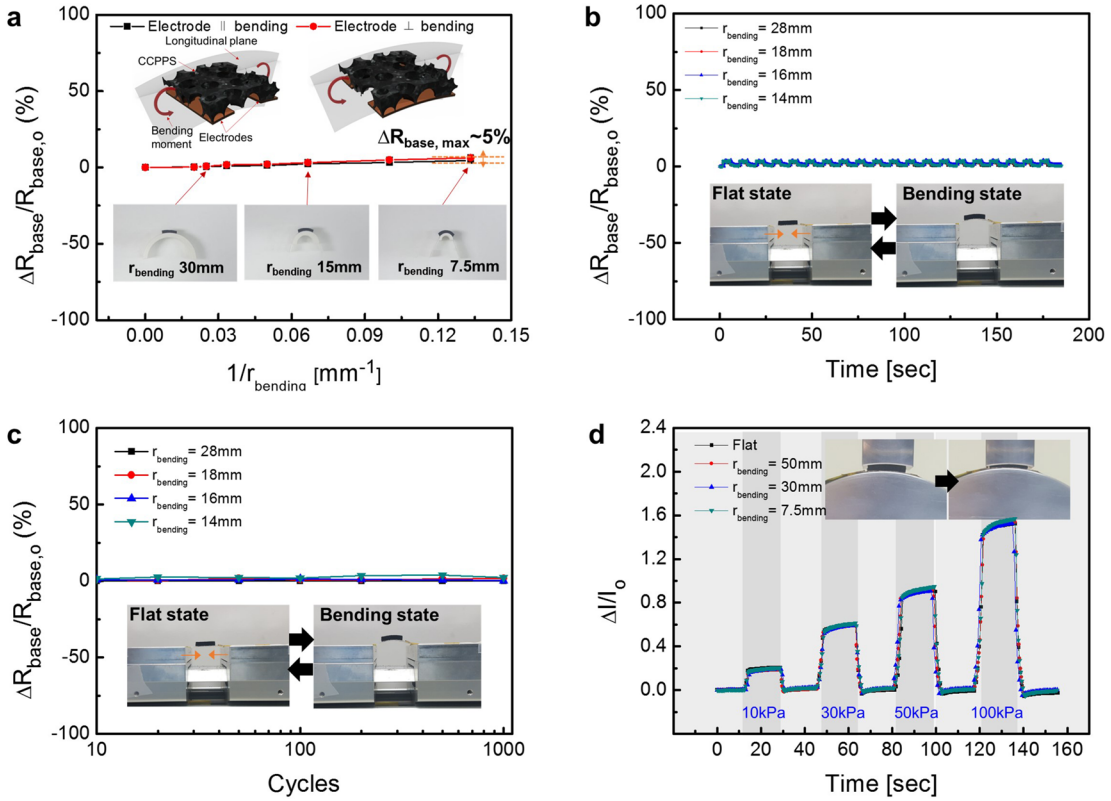

Figure 4. Bending insensitivity of a CCPPS-based flexible pressure sensor under bent conditions. (a) Change in the base resistance of the pressure sensor with various bending radii from 50 to 7.5 mm for both cases of electrodes||bending and electrodes⊥bending. (b) Recovery of the base resistance of the pressure sensor under repetitive dynamic bending cycles with different bending radii (28, 18, 16, and 14 mm). (c) Long-term reliability of the pressure sensor during 1000 bending cycles with different bending radii (28, 18, 16, and 14 mm). (d) Comparison of the dynamic pressure responses of the pressure sensor in bent (50, 30, and 7.5 mm) and flat states, showing bending-insensitive pressure sensing capability.

The pressure sensor can be used to detect different pressure levels with high resolution over wide ranges of pressures of $\lesssim$1 MPa. As shown in Figure 3d and Figure S4d, $\Delta I/I_0$ (blue curve) could instantly respond to input loads (black curve; measured by a load cell) with no remarkable time delays during step loading and step unloading. The response times ($\sim$8.5 ms for loading and $\sim$10 ms for unloading) were defined as a difference between the 90% rising times ($\Delta\tau_{90\%}$) of the two curves. The fast response of the pressure sensor facilitates a real-time pressure measurement under dynamic stimuli. Furthermore, the long-term reliability of pressure sensors is one of the important parameters for their use in practical applications. As shown in Figure 3e, the CCPPS-based pressure sensor exhibited excellent electromechanical reliability without noticeable instability or failures during 10000 repetitive compression/release cycles. In the magnified curves (inset), one can see that stable and repeatable responses were maintained after $\sim$8000 cycles. These results can offer the possibility of the CCPPS-based flexible pressure sensor monitoring dynamic human motions over an ultrawide pressure range.

As bending deformation can be applied to pressure sensors attached to human bodies, the flexible and wearable pressure sensors are required to exhibit electromechanical stability under both flat and curved surfaces. The effects of bending on the performance of the CCPPS-based flexible pressure sensor were investigated as shown in Figure 4. To evaluate the characteristics of bending insensitivity, the CCPPS-based pressure sensor was attached to the curved surfaces of supports with different bending radii ($r_{bending}$) that ranged from 50 to 7.5 mm as shown in Figure S5a. As shown in Figure 4a, for cases of electrodes||bending (i.e., the electrode pairs are aligned parallel to the longitudinal plane where opposite couple moments are acting) and electrodes⊥bending (i.e., the electrode pairs are aligned perpendicular to the longitudinal plane), the base resistance (R_{base}) remained almost constant at different values of $r_{bending}$ as shown in Figure 4a. The maximum normalized base resistance change ($\Delta R_{base}/R_{base,o}$) was measured to be within $\sim$5%. In Figure S5b, cross-sectional SEM images compare the microporous morphologies of the CCPPS with various values of $r_{bending}$. Despite the entire sensor structure being bent up to $r_{bending}$ of 7.5 mm, there was no significant current change due to negligible changes in contact between the CNT networks. The bending-insensitive property of the CCPPS was further verified by numerical simulation as shown in Figure S6. The cross section of the CCPPS was represented by a randomly distributed porous structure (micropore diameter of 300−500 μm, thickness of bridges of 50−100 μm), and the scale of the structure was modeled as the real size of the CCPPS-based pressure sensor. The bending-insensitive characteristics of the CCPPS originate from the nature of the microporous configuration. Because the change in the overall arrangement of the microporous structure accommodates the bending-induced deformation of the entire sensor structure, the deformations of individual micropores are reduced with no significant distortion of the PDMS bridges surrounding the micropores. The local strain of most of the PDMS bridges inside the sensor structure was measured to be $\lesssim$10% even

DOI: 10.1021/acsami.9b07636
ACS Appl. Mater. Interfaces XXXX, XXX, XXX−XXX

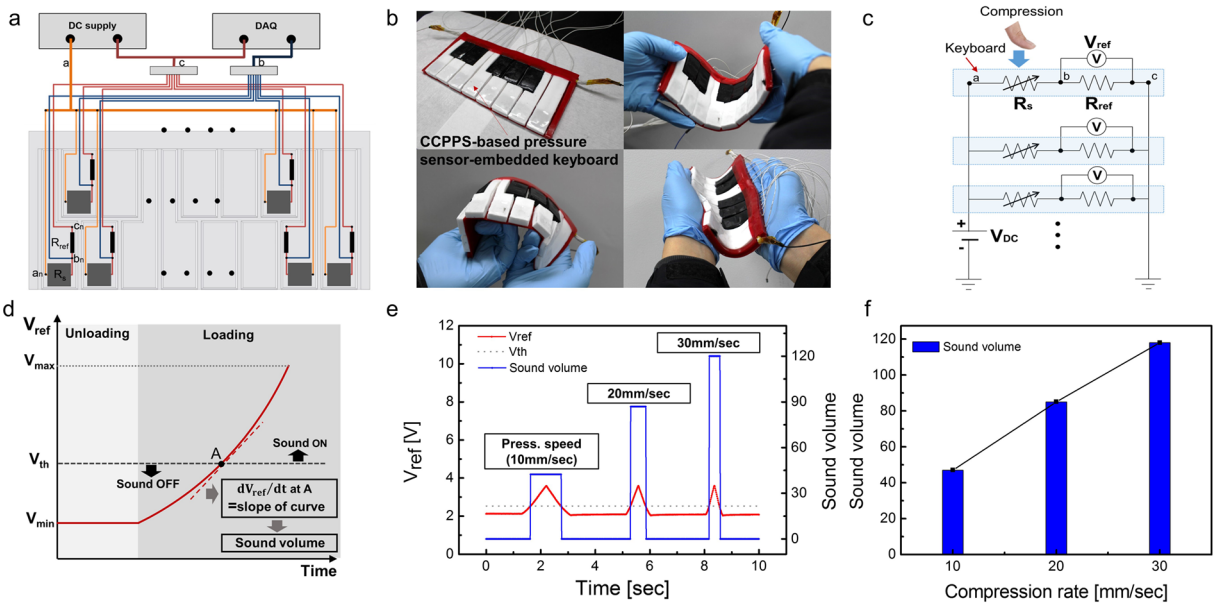

Figure 5. Flexible piano pad based on the CCPPS-based flexible pressure sensors, which mimics the principle of sound volume control of a real acoustic piano. (a) Schematic illustration of the overall system of the flexible piano pad composed of pressure sensor-embedded keyboards. (b) Photographic image of the fabricated flexible piano pad, showing its excellent flexibility and robustness. (c) Electrical circuits integrated into the keyboards for simultaneous measurement of the 13 multiple channels. (d) Method for the conversion of sensor signals to sound volumes. The slope of the voltage curve (dV_{ref}/dt) at point A is converted to the sound volume. (e and f) Sound volumes generated at different pressing speeds of the keyboard. As the pressing speed increased, the sound volume also linearly increased (47, 85, and 118 a.u. for 10, 20, and 30 mm/s, respectively).

when $r_{bending} \lesssim 5$ mm. Accordingly, contact between the micropores causing the current change does not noticeably occur under bent conditions. In addition, the reliability of CCPPS under dynamic bending stimulation was examined. In Figure 4b, the CCPPS-based pressure sensor was repeatedly bent to $r_{bending}$ values of 28, 18, 16, and 14 mm. During the first 20 bending cycles, the base resistance was almost completely returned to original values without a noticeable instability. The CCPPS-based pressure sensor showed excellent long-term reliability with a negligible change in R_{base} and no structural failure after 1000 bending/release cycles, as shown in Figure 4c. Moreover, the bending-insensitive pressure sensing capability of the CCPPS-based pressure sensor was investigated by comparing dynamic pressure responses under flat and bent conditions, as shown in Figure 4d. The responses at $r_{bending}$ values of 50, 30, and 7.5 mm were nearly identical to that of the flat condition, indicating that the pressure sensing performance of the sensor was not significantly affected by the bending-induced deformations. Such bending-insensitive pressure sensing capability enables the CCPPS-based flexible pressure sensor to accurately detect the normal forces or pressures even under bent situations in wearable human interface devices.

A flexible piano pad based on CCPPS-based flexible pressure sensor arrays was fabricated as a human interface device for an entertainment application. The flexible piano pad was designed to mimic the working principle of a real acoustic piano, where sound volumes can be controlled by the pressing speed of keyboards. Figure 5a shows a schematic illustration of a flexible piano pad, which is composed of 13 pressure sensor array-embedded keyboards. As shown in Figure 5b, the flexible piano pad exhibited excellent flexibility and robustness, because it was composed of a soft elastomer (Ecoflex 0030) and the CCPPS-based pressure sensors (detailed fabrication procedures are described in Figure S7a and the Experimental Section). Figure 5c shows a schematic illustration of voltage dividing circuits integrated within the keyboards for simultaneous measurement of 13 signals. Figure 5d shows a method for the conversion of voltage signals to sound volumes to implement mimicking of a real acoustic piano. When the pressure sensors within the keyboards are pressed by human fingers, reference voltages (V_{ref}) increase with decreasing resistances of the pressure sensors (R_s). When the value of V_{ref} reaches the threshold voltage (V_{th}) at point A, the slope of the curve (dV_{ref}/dt) at this point is converted to the sound volume. In addition, the sound was programmed to be turned on only when V_{ref} is higher than V_{th}. The sound volumes, which were simultaneously converted from 13 multiple channels, were output through the personal computer speaker as shown in Figure S7b. To evaluate the functionality, the sound volumes generated at different pressing speeds were compared. In Figure 5e, profiles of V_{ref} and the sound volume are represented by red and blue lines, respectively. It was clearly confirmed that as the pressing speed of the keyboards increased, an increased slope of the V_{ref} curve and increased sound volumes were produced (47, 85, and 118 a.u. for 10, 20, and 30 mm/s, respectively) with good linearity (Figure 5e,f). In addition, a variety of playing performances were evaluated by actually operating the flexible piano pad, as shown in Movie S4. In this video, the flexible piano pad obviously showed that the variation of sound volume depends on the pressing speeds of the human fingers. Also, it was able to be played at a very fast tempo corresponding to "prestissimo (beats per minute=200)" due to the fast response of the CCPPS-based pressure sensor. The flexible piano pad facilitated a series of musical chord implementations, when several keyboards were pressed at the same time. On the basis of this basic playing performance, the famous music "Doremi-Song" was successfully played.

DOI: 10.1021/acsami.9b07636
ACS Appl. Mater. Interfaces XXXX, XXX, XXX−XXX

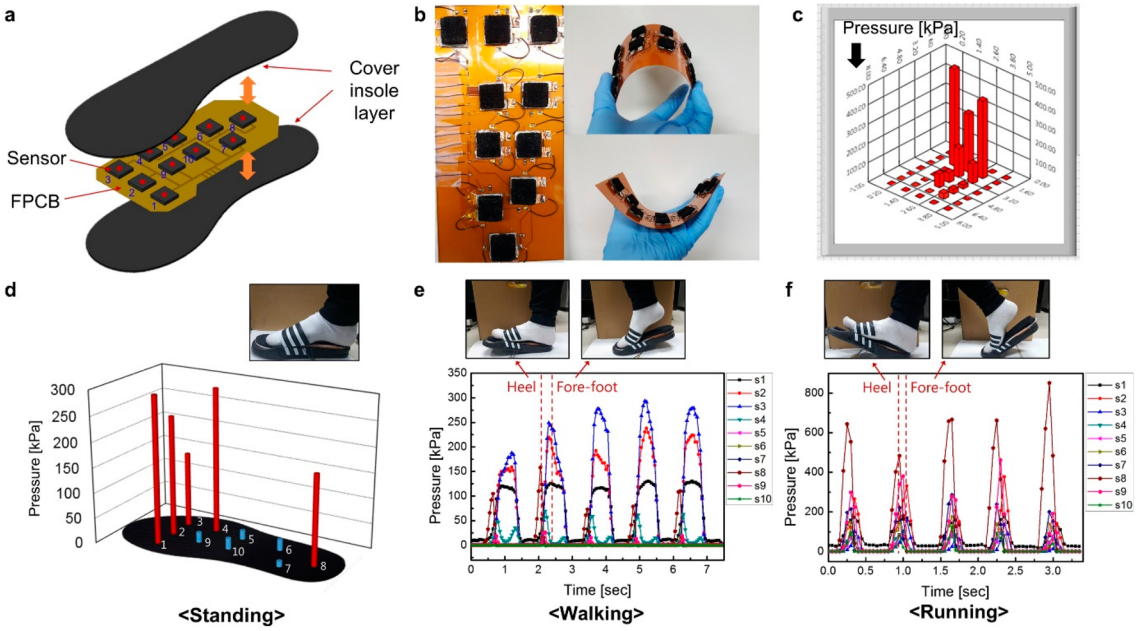

Figure 6. Flexible foot insole using the CCPPS-based flexible pressure sensors for real-time detection of the foot plantar pressure distribution. (a) Schematic illustration of the flexible foot insole. (b) Photographic images of the fabricated pressure sensor-integrated FPCB. (c) 3D mapping of the foot pressure distribution in the measurement system. (d) Foot plantar pressure distribution in a standing stance. (e and f) Dynamic changes of the pressures measured at each position during five steps of walking and running, respectively.

As a wearable healthcare monitoring device, an in-shoe type flexible foot insole using the CCPPS-based flexible pressure sensor arrays was fabricated for real-time monitoring of the foot plantar pressure distribution. Figure 6a displays a schematic illustration of the flexible foot insole. Ten CCPPS-based pressure sensor arrays were integrated on a flexible printed circuit board (FPCB) as shown Figure 6b. The pressure sensors were located on 10 critical positions, which support most of the body weights and adjust a body balance on foot anatomical areas:[38] fore-foot (1−3), midfoot (4, 5, 9, and 10), and heel (6−8). Individual sensors were packaged inside the sockets of a cover insole layer as depicted in Figure S8a. The two-bottom electrode configuration led to a stable connection of the pressure sensors on the electrical circuits of the FPCB. Also, the pressure sensors allowed accurate detection of local pressures without surrounding interference because the CCPPS does not suffer from the barreling effect under compressive loading. The voltage outputs generated from 10 pressure sensors were transferred to a data acquisition (DAQ) board and collected with a personal computer. In Figure 6c, the foot plantar pressure measured by each sensor was displayed at corresponding positions of a 3D bar graph in a measurement program. Movie S5 shows the real-time change of the foot plantar pressure distribution according to the posture changes of a human body. The output of this device was in the form of a "pressure" in the measurement program, as shown in Figure 6c and Movie S5. This could offer more user-friendly and direct information, compared with that of most of the previous studies where the output was simply in the form of an "electrical signal". To implement this function, voltage signals were converted to the pressure values by the following steps (Figure S8b). (1) V_{ref} values measured by the DAQ board were converted to $\Delta R/R_0$ using the equation $\Delta R/R_0 = (V_{in}/V_{ref} - 1) \times R_{ref}/R_0 - 1$. (2) $\Delta R/R_0$ values were converted to pressure values using calibration equations $P = f(\Delta R/R_0) = a \times \exp(b \times \Delta R/R_0)$ (a and b are fitting constants), derived from fitting the experimental data. The gait motion of a 70 kg tester, wearing a shoe with the flexible foot insole, was evaluated by measuring the foot plantar pressure distribution. Figure 6d shows the pressure distribution over the entire foot plantar area in a standing stance. 3D mapping clearly showed the pressure distribution related to the anatomical shape of the foot plantar. High pressures were observed in the region of the fore-foot (1−3) and the heel (8) primarily in contact with the insole, while relatively low pressures were measured in the midfoot part with an arch shape (5 and 10). Panels e and f of Figure 6 display continuous curves of the pressure values measured at each position during walking and running for five steps, respectively. In Figure 6e, a peak value of 8 was first observed, because the heel touched the ground at the beginning of the walking motions. In contrast, peak values of the fore-foot (1−3) were observed at the end of the walking motions. In Figure 6f, the peak values of all positions relatively increased with the time intervals between the peaks decreasing due to faster and more dynamic cyclic motions by running, compared with walking. Accordingly, the flexible foot insole based on the CCPPS-based pressure sensors was capable of collecting the static and dynamic pressure data of human gait motion, which can be applied to clinical or sports dynamics fields. The set of foot plantar pressure distribution data is one of the important indicators for diagnosing and treating patients with diseases like obesity, diabetes, spinal diseases, etc.[38−40] Furthermore, this technique can be used to assess athletic performance or rehabilitation by analyzing the gait patterns and speeds of athletes.

CONCLUSION

In summary, we developed a thin CCPPS-based flexible pressure sensor, which is capable of the ultrawide pressure-range and bending-insensitive pressure sensing. Because of the gradual change in the contact between the CNT networks

DOI: 10.1021/acsami.9b07636
ACS Appl. Mater. Interfaces XXXX, XXX, XXX−XXX

deposited on the micropores up to high compressive strain of the CCPPS, the pressure sensor operated in a very wide range from ultralow to high pressures (10 Pa to 1.2 MPa), with favorable sensitivity and high linearity maintained. Also, the CCPPS-based pressure sensor showed low hysteresis, fast dynamic responses, and long-term reliability due to the reversible and fully restored closure/opening of the micropores. The bending-insensitive pressure sensing capability of the CCPPS-based pressure sensor facilitates the accurate and stable detection of normal pressure under bent conditions. Accordingly, the thin CCPPS-based pressure sensor could be utilized for human interface devices for entertainment and healthcare monitoring applications. In the future, our technology might be integrated with a wireless system for a variety of applications, including portable human−machine interface devices, prosthetic skins, and mobile healthcare systems. Moreover, we expect that the pressure sensing parameters could be precisely controlled and optimized by tuning the porosity, arrangement, and size of the micropores of the CCPPS for a variety of wearable sensing applications.

EXPERIMENTAL SECTION

Preparation of a CNT Network-Coated Porous PDMS Sponge (CCPPS). A sugar template (15 mm × 15 mm × 15 mm) was immersed in a degassed polydimethylsiloxane prepolymer (PDMS, Sylgard 184, Dow Corning Co., 10:1 matrix:curing agent mass ratio). The liquid PDMS prepolymer was infiltrated into the sugar template in a vacuum chamber for 1 h and then cured in a convection oven at 70 °C for 2 h. The composite of sugar and cured PDMS was cut into a thin slice with a thickness of ∼3 mm using sandpaper and immersed in deionized water at 60 °C for 1 h to dissolve the sugar portion for the fabrication of a porous PDMS sponge (PPS, 15 mm × 15 mm × 3 mm). Then, the obtained PPS was treated with an oxygen plasma for 10 min; 0.25 g of multiwalled carbon nanotubes (MWCNTs) (Hyosung, diameter of 16 ± 3.6 nm, length of 5−20 μm) was dispersed in 100 mL of isopropyl alcohol (IPA). After vortex mixing for 1 h, ultrasonication was carried out for 1 h to prepare a homogeneous 0.25 wt % CNT-IPA dispersion. The plasma-treated PPS was immersed in the CNT-IPA dispersion and repeatedly squeezed for CNT coating on the surfaces of the PDMS backbone. After complete evaporation of the IPA solvent, the prepared CCPPS was rinsed in deionized water and dried in a convection oven at 50 °C for 1 h. The resistance of the fabricated CCPPS was lower than ∼3 kΩ. For comparison, a 0.3 wt % CNT-embedded solid PDMS (15 mm × 15 mm × 3 mm), which has a resistance level similar to that of the CCPPS, was also fabricated. The MWCNTs were mixed with the PDMS prepolymer (0.3:99.7 MWCNT:PDMS mass ratio) using a planetary centrifugal mixer (ARE-310, Thinky) to prepare a homogeneous mixture. After the PDMS prepolymer had been cured in a convection oven at 70 °C for 2 h, a CNT-embedded PDMS was fabricated.

Preparation of a CCPPS-Based Pressure Sensor. Two flexible copper sheets (thickness of ∼50 μm) were attached on a flexible polyethylene terephthalate film (PET, thickness of ∼50 μm) for the fabrication of two bottom electrodes. The CCPPS was bonded to the electrodes using a silver paste adhesive to prepare a CCPPS-based pressure sensor. Then, the silver paste was annealed in a convection oven at 120 °C for 30 min.

Characterization of a CCPPS-Based Pressure Sensor. The surface and cross-sectional morphology of the CCPPS were characterized by field emission scanning electron microscopy (FE-SEM, Sirion, FEI) and optical microscopy (VH-Z100R, Keyence). The internal cross-sectional geometries of the CCPPS were investigated using nondestructive micro computed tomography (Micro CT, SKYSCAN 1272, Bruker). A tensile/compression testing machine (C224-E053D Autograph AG-X Plus, Shimadzu) capable of the precise control of load and displacement was used to characterize pressure responses of the CCPPS-based pressure sensor. Force and electrical current data were collected using a load cell (Load Cell SLBL, Shimadzu) and a source meter (Keithley 2400, Keithley Instruments), respectively. During the characterization of the CCPPS, a bias voltage of 1 V was applied.

Preparation of a 1D Sensor Array. The CCPPS was cut into a width of 7 mm (7 mm × 7 mm × 3 mm) using a razor blade. Copper electrodes and interconnects were attached on a polyimide film (thickness of ∼50 μm), and six CCPPSs were bonded to the copper electrodes to form a 1D spatial array. The gap between the adjacent sensors was designed to be <1 mm. The electrical circuits were connected to a data acquisition (DAQ) board.

Preparation of a Flexible Piano Pad. At first, piano keyboard-shaped molds, which have empty spaces (15 mm × 15 mm × 3 mm), were manufactured using a 3D printer. The Ecoflex prepolymer (Ecoflex 0030, Smooth-On, 1:1 matrix A:matrix B mass ratio) was poured into the molds and cured in a convection oven at 80 °C for 2 h, for the formation of the keyboard housings. A voltage dividing circuit consisting of the CCPPS-based pressure sensor and a reference resistance was integrated into an empty space of each keyboard housing for the preparation of 13 keyboard components (eight white keys and five black keys, from Do; C4 to Do; C5). Each keyboard component was bonded in an array configuration using a silicone adhesive to form a flexible piano pad. The electrical circuits were connected to the DAQ board and PC where sound midi files were programmed.

Preparation of a Flexible Foot Insole. Ten CCPPS-based pressure sensors were attached on a flexible printed circuit board (FPCB, thickness of ∼100 μm) using an adhesive tape (136 ROK, 3M Corp.). Then, the electrical wires connected to the electrode pairs were bonded to the exposed parts of the electrical circuit of the FPCB using a soldering process. Chip type resistors were also bonded to the electrical circuit by soldering. The sensor-integrated FPCB was combined with a cover insole layer with socket structures for completion of a flexible foot insole. The electrical circuits were connected to a DAQ board and PC where real-time 3D mapping was programmed for real-time measurement.

ASSOCIATED CONTENT

Supporting Information

The Supporting Information is available free of charge on the ACS Publications website at DOI: 10.1021/acsami.9b07636.

SEM and optical analysis of compressive behavior of a CNT-coated porous elastomer sponge (CCPPS), calculation of the porosity of the CCPPS, simulation analysis of bending of the CCPPS, Table S1, and Figures S1−S8 (PDF)

Micro computed tomography movie of the internal geometry of the CCPPS (MP4)

Gradual geometrical change of the microporous configuration of the CCPPS (MP4)

Demonstration of a 1D sensor array (MP4)

Demonstration of a playing performance of a flexible piano pad device (MP4)

Demonstration of a real-time 3D plotting of the foot pressure distribution (MP4)

AUTHOR INFORMATION

Corresponding Authors

*E-mail: inkyu@kaist.ac.kr.

*E-mail: oyongsuk@kaist.ac.kr.

ORCID

Morteza Amjadi: 0000-0003-2907-5025

Taek-Soo Kim: 0000-0002-2825-7778

Inkyu Park: 0000-0001-5761-7739

DOI: 10.1021/acsami.9b07636
ACS Appl. Mater. Interfaces XXXX, XXX, XXX−XXX

Notes

The authors declare no competing financial interest.

■ ACKNOWLEDGMENTS

This work was supported by the following research grants: (1) the convergence technology development program for bionic arm through the National Research Foundation of Korea (NRF) funded by the Ministry of Science & ICT (2017M3C1B2085318) and (2) a National Research Foundation of Korea (NRF) grant funded by the Korean Government (MSIP) (2015R1A5A1037668).

■ REFERENCES

(1) Someya, T.; Sekitani, T.; Iba, S.; Kato, Y.; Kawaguchi, H.; Sakurai, T. A Large-Area, Flexible Pressure Sensor Matrix with Organic Field-Effect Transistors for Artificial Skin Applications. *Proc. Natl. Acad. Sci. U. S. A.* **2004**, *101*, 9966−9970.

(2) Takei, K.; Takahashi, T.; Ho, J. C.; Ko, H.; Gillies, A. G.; Leu, P. W.; Fearing, R. S.; Javey, A. Nanowire Active-Matrix Circuitry for Low-Voltage Macroscale Artificial Skin. *Nat. Mater.* **2010**, *9*, 821−826.

(3) Hammock, M. L.; Chortos, A.; Tee, B. C. K.; Tok, J. B. H.; Bao, Z. 25th Anniversary Article: The Evolution of Electronic Skin (E-Skin): A Brief History, Design Considerations, and Recent Progress. *Adv. Mater.* **2013**, *25*, 5997−6038.

(4) Wang, X.; Dong, L.; Zhang, H.; Yu, R.; Pan, C.; Wang, Z. L. Recent Progress in Electronic Skin. *Adv. Sci.* **2015**, *2*, 1500169.

(5) Bauer, S.; Bauer-Gogonea, S.; Graz, I.; Kaltenbrunner, M.; Keplinger, C.; Schwödiauer, R. 25th Anniversary Article: A Soft Future: From Robots and Sensor Skin to Energy Harvesters. *Adv. Mater.* **2014**, *26*, 149−162.

(6) Trivedi, D.; Rahn, C. D.; Kier, W. M.; Walker, I. D. Soft Robotics: Biological Inspiration, State of the Art, and Future Research. *Applied Bionics and Biomechanics* **2008**, *5*, 99−117.

(7) Lee, H.; Kwon, D.; Cho, H.; Park, I.; Kim, J. Soft Nanocomposite Based Multi-Point, Multi-Directional Strain Mapping Sensor Using Anisotropic Electrical Impedance Tomography. *Sci. Rep.* **2017**, *7*, 39837.

(8) Schwartz, G.; Tee, B. C. K.; Mei, J.; Appleton, A. L.; Kim, D. H.; Wang, H.; Bao, Z. Flexible Polymer Transistors with High Pressure Sensitivity for Application in Electronic Skin and Health Monitoring. *Nat. Commun.* **2013**, *4*, 1858−1859.

(9) Boutry, C. M.; Nguyen, A.; Lawal, Q. O.; Chortos, A.; Rondeau-Gagné, S.; Bao, Z. A Sensitive and Biodegradable Pressure Sensor Array for Cardiovascular Monitoring. *Adv. Mater.* **2015**, *27*, 6954−6961.

(10) Zang, Y.; Zhang, F.; Di, C. A.; Zhu, D. Advances of Flexible Pressure Sensors toward Artificial Intelligence and Health Care Applications. *Mater. Horiz.* **2015**, *2*, 140−156.

(11) Kwon, D.; Lee, T. I.; Shim, J.; Ryu, S.; Kim, M. S.; Kim, S.; Kim, T. S.; Park, I. Highly Sensitive, Flexible, and Wearable Pressure Sensor Based on a Giant Piezocapacitive Effect of Three-Dimensional Microporous Elastomeric Dielectric Layer. *ACS Appl. Mater. Interfaces* **2016**, *8*, 16922−16931.

(12) Yang, Y.; Zhang, H.; Lin, Z. H.; Zhou, Y. S.; Jing, Q.; Su, Y.; Yang, J.; Chen, J.; Hu, C.; Wang, Z. L. Human Skin Based Triboelectric Nanogenerators for Harvesting Biomechanical Energy and as Self-Powered Active Tactile Sensor System. *ACS Nano* **2013**, *7*, 9213−9222.

(13) Zhu, G.; Yang, W. Q.; Zhang, T.; Jing, Q.; Chen, J.; Zhou, Y. S.; Bai, P.; Wang, Z. L. Self-Powered, Ultrasensitive, Flexible Tactile Sensors Based on Contact Electrification. *Nano Lett.* **2014**, *14*, 3208−3213.

(14) Wang, S.; Lin, L.; Wang, Z. L. Triboelectric Nanogenerators as Self-Powered Active Sensors. *Nano Energy* **2015**, *11*, 436−462.

(15) Takamatsu, S.; Yamashita, T.; Imai, T.; Itoh, T. Lightweight Flexible Keyboard with a Conductive Polymer-Based Touch Sensor Fabric. *Sens. Actuators, A* **2014**, *220*, 153−158.

(16) Lipomi, D. J.; Vosgueritchian, M.; Tee, B. C. K.; Hellstrom, S. L.; Lee, J. A.; Fox, C. H.; Bao, Z. Skin-like Pressure and Strain Sensors Based on Transparent Elastic Films of Carbon Nanotubes. *Nat. Nanotechnol.* **2011**, *6*, 788−792.

(17) Mannsfeld, S. C. B.; Tee, B. C.-K.; Stoltenberg, R. M.; Chen, C. V. H.-H.; Barman, S.; Muir, B. V. O.; Sokolov, A. N.; Reese, C.; Bao, Z. Highly Sensitive Flexible Pressure Sensors with Microstructured Rubber Dielectric Layers. *Nat. Mater.* **2010**, *9*, 859−864.

(18) Xiao, X.; Yuan, L.; Zhong, J.; Ding, T.; Liu, Y.; Cai, Z.; Rong, Y.; Han, H.; Zhou, J.; Wang, Z. L. High-Strain Sensors Based on ZnO Nanowire/Polystyrene Hybridized Flexible Films. *Adv. Mater.* **2011**, *23*, 5440−5444.

(19) Lozano-Pérez, C.; Cauich-Rodríguez, J. V.; Avilés, F. Influence of Rigid Segment and Carbon Nanotube Concentration on the Cyclic Piezoresistive and Hysteretic Behavior of Multiwall Carbon Nanotube/Segmented Polyurethane Composites. *Compos. Sci. Technol.* **2016**, *128*, 25−32.

(20) Zhang, R.; Deng, H.; Valenca, R.; Jin, J.; Fu, Q.; Bilotti, E.; Peijs, T. Strain Sensing Behaviour of Elastomeric Composite Films Containing Carbon Nanotubes under Cyclic Loading. *Compos. Sci. Technol.* **2013**, *74*, 1−5.

(21) Choong, C. L.; Shim, M. B.; Lee, B. S.; Jeon, S.; Ko, D. S.; Kang, T. H.; Bae, J.; Lee, S. H.; Byun, K. E.; Im, J.; Jeong, Y. J.; Park, C. E.; Park, J.-J.; Chung, U.-I. Highly Stretchable Resistive Pressure Sensors Using a Conductive Elastomeric Composite on a Micropyramid Array. *Adv. Mater.* **2014**, *26*, 3451−3458.

(22) Qi, K.; He, J.; Wang, H.; Zhou, Y.; You, X.; Nan, N.; Shao, W.; Wang, L.; Ding, B.; Cui, S. A Highly Stretchable Nanofiber-Based Electronic Skin with Pressure-, Strain-, and Flexion-Sensitive Properties for Health and Motion Monitoring. *ACS Appl. Mater. Interfaces* **2017**, *9*, 42951−42960.

(23) Pang, C.; Lee, G. Y.; Kim, T. Il; Kim, S. M.; Kim, H. N.; Ahn, S. H.; Suh, K. Y. A Flexible and Highly Sensitive Strain-Gauge Sensor Using Reversible Interlocking of Nanofibres. *Nat. Mater.* **2012**, *11*, 795−801.

(24) Wang, X.; Gu, Y.; Xiong, Z.; Cui, Z.; Zhang, T. Silk-Molded Flexible, Ultrasensitive, and Highly Stable Electronic Skin for Monitoring Human Physiological Signals. *Adv. Mater.* **2014**, *26*, 1336−1342.

(25) Yu, G.; Hu, J.; Tan, J.; Gao, Y.; Lu, Y.; Xuan, F. A Wearable Pressure Sensor Based on Ultra-Violet/Ozone Microstructured Carbon Nanotube/Polydimethylsiloxane Arrays for Electronic Skins. *Nanotechnology* **2018**, *29*, 115502.

(26) Lu, C.; Gao, Y.; Yu, G.; Xu, M.; Tan, J.; Xuan, F. Laser-Microengineered Flexible Electrodes with Enhanced Sensitivity for Wearable Pressure Sensors. *Sens. Actuators, A* **2018**, *281*, 124−129.

(27) Xu, M.; Gao, Y.; Yu, G.; Lu, C.; Tan, J.; Xuan, F. Flexible Pressure Sensor Using Carbon Nanotube-Wrapped Polydimethylsiloxane Microspheres for Tactile Sensing. *Sens. Actuators, A* **2018**, *284*, 260−265.

(28) Tai, Y.; Mulle, M.; Aguilar Ventura, I.; Lubineau, G. A Highly Sensitive, Low-Cost, Wearable Pressure Sensor Based on Conductive Hydrogel Spheres. *Nanoscale* **2015**, *7*, 14766−14773.

(29) Gong, S.; Schwalb, W.; Wang, Y.; Chen, Y.; Tang, Y.; Si, J.; Shirinzadeh, B.; Cheng, W. A Wearable and Highly Sensitive Pressure Sensor with Ultrathin Gold Nanowires. *Nat. Commun.* **2014**, *5*, 3132.

(30) Yao, H.-B.; Ge, J.; Wang, C. F.; Wang, X.; Hu, W.; Zheng, Z. J.; Ni, Y.; Yu, S. H. A Flexible and Highly Pressure-Sensitive Graphene-Polyurethane Sponge Based on Fractured Microstructure Design. *Adv. Mater.* **2013**, *25*, 6692−6698.

(31) Pang, Y.; Tian, H.; Tao, L.; Li, Y.; Wang, X.; Deng, N.; Yang, Y.; Ren, T. L. Flexible, Highly Sensitive, and Wearable Pressure and Strain Sensors with Graphene Porous Network Structure. *ACS Appl. Mater. Interfaces* **2016**, *8*, 26458−26462.

(32) Zhang, H.; Liu, N.; Shi, Y.; Liu, W.; Yue, Y.; Wang, S.; Ma, Y.; Wen, L.; Li, L.; Long, F.; Zou, Z.; Gao, Y. Piezoresistive Sensor with High Elasticity Based on 3D Hybrid Network of Sponge@CNTs@Ag NPs. *ACS Appl. Mater. Interfaces* **2016**, *8*, 22374−22381.

DOI: 10.1021/acsami.9b07636
ACS Appl. Mater. Interfaces XXXX, XXX, XXX−XXX

(33) Han, J. W.; Kim, B.; Li, J.; Meyyappan, M. Flexible, Compressible, Hydrophobic, Floatable, and Conductive Carbon Nanotube-Polymer Sponge. *Appl. Phys. Lett.* **2013**, *102*, 051903.
(34) Iglio, R.; Mariani, S.; Robbiano, V.; Strambini, L.; Barillaro, G. Flexible Polydimethylsiloxane Foams Decorated with Multiwalled Carbon Nanotubes Enable Unprecedented Detection of Ultralow Strain and Pressure Coupled with a Large Working Range. *ACS Appl. Mater. Interfaces* **2018**, *10*, 13877−13885.
(35) Lee, S.; Reuveny, A.; Reeder, J.; Lee, S.; Jin, H.; Liu, Q.; Yokota, T.; Sekitani, T.; Isoyama, T.; Abe, Y.; Suo, Z.; Someya, T. A Transparent Bending-Insensitive Pressure Sensor. *Nat. Nanotechnol.* **2016**, *11*, 472−478.
(36) Chen, S.; Zhuo, B.; Guo, X. Large Area One-Step Facile Processing of Microstructured Elastomeric Dielectric Film for High Sensitivity and Durable Sensing over Wide Pressure Range. *ACS Appl. Mater. Interfaces* **2016**, *8*, 20364−20370.
(37) Graz, I.; Krause, M.; Bauer-Gogonea, S.; Bauer, S.; Lacour, S. P.; Ploss, B.; Zirkl, M.; Stadlober, B.; Wagner, S. Flexible Active-Matrix Cells with Selectively Poled Bifunctional Polymer-Ceramic Nanocomposite for Pressure and Temperature Sensing Skin. *J. Appl. Phys.* **2009**, *106*, 034503.
(38) Abdul Razak, A. H.; Zayegh, A.; Begg, R. K.; Wahab, Y. Foot Plantar Pressure Measurement System: A Review. *Sensors* **2012**, *12*, 9884−9912.
(39) Hills, A. P.; H, E. M. Plantar Pressure Differences between Obese and Non-Obese Adults: A Biomechanical Analysis. *Int. J. Obes.* **2001**, *25*, 1674−1679.
(40) Paton, J.; Bruce, G.; Jones, R.; Stenhouse, E. Effectiveness of Insoles Used for the Prevention of Ulceration in the Neuropathic Diabetic Foot: A Systematic Review. *J. Diabetes Complications* **2011**, *25*, 52−62.

DOI: 10.1021/acsami.9b07636
ACS Appl. Mater. Interfaces XXXX, XXX, XXX−XXX